Is a single late SPECT/CT based kidney 177Lu-dosimetry superior to hybrid dosimetry with sequential multiple time-point whole-body planar scans in combination with an early SPECT/CT?

Beykan, Seval; Tran-Gia, Johannes; Borup Jensen, Svend; Lassmann, Michael

Published in:
Physica Medica

DOI (link to publication from Publisher):
10.1016/j.ejmp.2022.06.002

Publication date:
2022

Document Version
Publisher's PDF, also known as Version of record

Physica Medica 100 (2022) 39–50

Contents lists available at ScienceDirect

Physica Medica

journal homepage: www.elsevier.com/locate/ejmp

Is a single late SPECT/CT based kidney ^{177}Lu-dosimetry superior to hybrid dosimetry with sequential multiple time-point whole-body planar scans in combination with an early SPECT/CT?

Seval Beykan [a,*], Johannes Tran-Gia [a], Svend Borup Jensen [b,c], Michael Lassmann [a]

[a] Department of Nuclear Medicine, University of Würzburg, Würzburg, Germany
[b] Department of Nuclear Medicine, Aalborg University Hospital, Aalborg, Denmark
[c] Department of Chemistry and Bioscience, Aalborg University, Aalborg, Denmark

ARTICLE INFO

Keywords:
^{177}Lu dosimetry
Multiple time-point SPECT/CT dosimetry
Single time-point SPECT/CT dosimetry
Hybrid planar/SPECT/CT dosimetry

ABSTRACT

Purpose: The aim is to assess the impact of different imaging-protocols on image-based kidney dosimetry in ^{177}Lu labelled peptide receptor radiotherapies.
Methods: Kidney data of five [^{177}Lu]Lu-OPS201 injected pigs and a 3D printed phantom were used for comparing the absorbed doses and time-integrated activity coefficients calculated based on the following imaging-protocols: A-) multiple time-point SPECT/CTs, B-) multiple time-point planar scans in combination with one SPECT/CT, C-) single time-point SPECT/CT. In addition, the influence of late scan time-points on kidney dosimetry was investigated by sequentially eliminating scan data at $>$ 100 h from the pig/phantom datasets for imaging-protocols A and B.
Results: Compared to imaging-protocol A, absorbed doses based on imaging-protocols B and C (scans at $>$ 24 h post-injection) were always lower (differences $>$ 34%). The best agreement in absorbed dose was achieved by imaging-protocol C at $\sim$ 100 h post-injection (difference: 4%). Regarding the phantom/pig experiments, eliminating scan data at $>$ 100 h post-injection increased the time-integrated activity coefficients calculated based on imaging-protocols A and B by up to 83%.
Conclusion: While imaging-protocol A is accurate if scans at $>\sim$100 h are included, it is time-consuming. In addition to being time-consuming, imaging-protocol B shows high differences associated with organ-count overlay, a lack of accuracy concerning the geometric mean based 2D attenuation correction, and 2D background subtraction due to the inhomogeneous and time-varying background contributions. Our findings indicate that dosimetry based on imaging-protocol C, if appropriately performed, provides similar kidney absorbed doses compared to imaging-protocol A, while only a single scan time-point is necessary.

Introduction

The essential role of patient-specific treatment planning and activity administration or, in other words, dosimetry was discoursed in several publications not only for treatment outcome but also to prevent toxicity in ^{177}Lu-labelled peptide receptor radionuclide treatments [1–8]. There are also several clinical studies on ^{177}Lu-labelled compounds that provide absorbed doses (ADs) and emphasize the necessity and importance of dosimetry [9–12]. For instance, the correlation between tumor absorbed doses and the response to the treatment was reported for

Abbreviations: AD, absorbed Dose; ADC, Total acquisition duration of the SPECT scan post-injection; A(r_s,t), Activity in selected region as a function of time after the administration; CT, Computed tomography; CV, Coefficient of variation; D(r_s), Total absorbed dose to the tissue under investigations by self-irradiation; ^{177}Lu, Lutetium-177; Imaging-protocol A, Multiple time-point SPECT/CT imaging; Imaging-protocol B, Multiple time-point planar scans in combination with one SPECT/CT imaging; Imaging-protocol C, Single time-point SPECT/CT imaging; OPS201, Satoreotide-tetraxetan, DOTA-JR11; PI, Post-injection; ROI, Region of interest; r_s, The tissue under investigations; S($r_s \leftarrow r_s$), Absorbed dose per decay or the dose rate per unit activity; Scan-tps, Scan time-points; SPECT, Single-photon emission computed tomography; SD, Standard deviation; TAC, Percentage uptake versus time curve; t, The SPECT/CT scan time-points post-injection; T_{eff}, Effective half-life; TC, Total number of counts in the drawn region; TIAC, Time-integrated activity coefficient; VOI, Volume of interest.

* Corresponding author at: Department of Nuclear Medicine, University Hospital Würzburg, Oberdürrbacher Str. 6, 97080 Würzburg, Germany.
E-mail address: Beykan_s@ukw.de (S. Beykan).

https://doi.org/10.1016/j.ejmp.2022.06.002
Received 31 August 2021; Received in revised form 25 May 2022; Accepted 11 June 2022
Available online 17 June 2022

patients with pancreatic neuroendocrine tumors and clinical benefits were discussed by Ilan E, et al. [13]. In addition, Sundlov, et al. [8] (with 51 patients), Garske-Roman, et al. [5] (with 200 patients), and Del Petre, et al. [1] (with 52 patients) published their SPECT/CT based dosimetry studies and showed that the suggested 4 × 7.4 GBq ^{177}Lu-labelled peptide receptor radionuclide treatment undertreated 73%, 49%, and 85% of the patients, respectively [14]. They mentioned that with patient-specific treatment planning, not only the treatment responses but also the safety of the patients (e.g., regarding kidney toxicity) could be improved.

The European Council Directive 2013/59/Euratom/Article 56 states that 'For all medical exposure of patients for radiotherapeutic purposes, exposures of target volumes shall be individually planned and their delivery appropriately verified taking into account that doses to non-target volumes and tissues shall be as low as reasonably achievable and consistent with the intended radiotherapeutic purpose of the exposure.' The member states had to put into force the laws and regulations necessary to comply with the basic safety standards by at latest 6 February 2018 (cf. Art. 106 of the basic safety standards) [15]. Although in the European Council Directive 2013/59/Euratom/Article 56, dosimetry is cited as compulsory for all radiopharmaceutical applications, in the currect published EANM position paper on article 56 of the Council Directive 2013/59/Euratom [16], dosimetry is cited as either optional (e.g. for [^{177}Lu]Lu-DOTATATE) or advisable (e.g. for other ^{177}Lu-labelled somatostatin receptor ligands). Satoreotide-tetraxetan (OPS, DOTA-JR11) is a newly developed somatostatin receptor antagonist and its combination with ^{177}Lu ([^{177}Lu]Lu-OPS201) is used for the treatments of neuroendocrine tumors and gastroenteropancreatic neuroendocrine tumors. Based on the limited number of head-to-head comparisons of somatostatin receptor antagonists and agonists, previous preclinical and clinical studies have indicated that radiolabeled OPS201 antagonist are superior to the corresponding agonists (such as DOTATATE and DOTATOC), especially regarding tumor targeting despite little to no internalization in tumor cells [12,17–19].

For the studies with [^{177}Lu]Lu-OPS201, performing dosimetry is classified as compulsory and advisable according to the European Council Directive 2013/59/Euratom [15] and the current EANM position paper [16], respectively.

Dosimetry is a concept of verifying ADs (e.g. for organs-at-risk or tumors) or determining the required treatment activity [6]. For ^{177}Lu-labelled somatostatin receptor therapies applied to the patients with neuroendocrine tumors in nuclear medicine, the kidneys (23 Gy) and the bone marrow (2 Gy) are organs-at-risk [17,20]. Therefore, kidney and bone marrow dosimetry are main focuses for the ^{177}Lu-labelled therapeutic applications for the patients with neuroendocrine tumors. In general, the steps of organ/tumor dosimetry for ^{177}Lu-based studies can be summarized as follows: quantitative imaging, creation of time-activity curves or percentage uptake versus time curves (TACs) per organ/tumor, calculation of time-integrated activity coefficients (TIACs), and dose calculations for each organ/tumor. Each of these steps needs to be analyzed and evaluated carefully for reliable and accurate dose calculations. Proposed image datasets required for dosimetry include multiple sequential 3D (SPECT/CT or PET/CT) or 2D (whole-body planar) scans acquired post-injection. Alternatively, dosimetry based on multiple sequential 2D scans (whole-body planar) in combination with a single 3D scan (SPECT/CT) [21,22], or even based on only a single SPECT/CT acquisition have been proposed [23].

Depending on the chosen imaging method, over- or underestimations of ADs can be observed. Over- or underestimation of ADs in dosimetry are typically associated with organ-count overlays as well as errors in volume determination, 2D attenuation correction, and 2D background subtraction for 2D based calculations [24]. Multiple time-point SPECT/CT imaging based dosimetry (imaging-protocol A) is considered as the most accurate dosimetry method and, therefore, the gold standard for dosimetry [25]. However, it is time-consuming for staff and causing discomfort to the patient, and might, therefore, be difficult to integrate into the clinical routine. Multiple time-point whole-body planar scans in combination with one SPECT/CT dosimetry (hybrid method, imaging-protocol B) is mainly considered a less time-consuming alternative to imaging-protocol A since the total acquisition duration required for the imaging-protocol B is shorter compared to imaging-protocol A. Another less time-consuming potential alternative, published by Hänscheid et al. [23], is single time-point SPECT/CT imaging based dosimetry (imaging-protocol C).

Up to now, there is no published study showing a head-to-head comparison of kidney dosimetry results (TIACs and absorbed doses) between the imaging-protocol A, B and C. To fulfill this gap, the main goal of this study is to find a more practical and reasonably accurate alternative [23] for performing dosimetry instead of the time-consuming imaging-protocol A approach. For this purpose, the right kidney TIACs and the corresponding ADs of five [^{177}Lu]Lu-OPS201 injected pigs were calculated and compared based on three different imaging protocols (imaging-protocol A, B and C).

Similar to the choice of imaging modality, the choice of scan time-points (scan-tps) PI is another crucial influencing factor for dosimetry [18,26]. The scan-tps PI must be selected based on physical and chemical properties of the administered radionuclide and peptide analog. The early scan-tps PI (at $<$ 24 h PI for the ^{177}Lu-labelled somatostatin receptor ligands) provide valuable information related to the uptake pattern of the radiopharmaceutical's biodistribution [26]. In contrast, the late scan-tps PI (at $>$ 72 h PI for the ^{177}Lu-labelled somatostatin receptor ligands) provide essential information on the radiopharmaceutical's retention, and, therefore, have a considerable impact on the TIAC calculation, which directly affects the absorbed doses [18]. Until today, neither the required number of scan-tps PI nor the required time interval concerning scan-tp PI are optimized for the dosimetry of ^{177}Lu-labelled somatostatin receptor studies [21]. In addition, there is no published study investigating the effect of late follow up scan-tps PI neither on the imaging-protocol A nor on the imaging-protocol B including head-to-head TIAC comparisons. Therefore, as a second goal of this study, we investigated the effect of late scan-tps PI on the TIACs by using one of the pig datasets. In addition to the pig data, a fabricated 3D printed phantom mimicking the biokinetics of the selected pig was used to verify our observations under precisely known conditions. The kidney TIACs of the pig (the one with the highest number of scan-tps PI) and the phantom were calculated separately by using different combinations of scan-tps PI. This investigation was performed for both the imaging-protocol A and B. The resulting right kidney TIACs of the pigs were compared to evaluate the effect of using late scan-tps PI on the dosimetry. For an unbiased assessment, we repeated the analysis by using a manufactured 3D printed kidney phantom (mimicking the biokinetics of pig 1).

Methods

The OPS201 (Satoreotide-tetraxetan, DOTA-JR11) synthesis and labelling including the [^{177}Lu]Lu-OPS201 administration of the pigs (3 females and 2 males, age: ~3 months, weight: 28 ± 2 kg, administered activity: 97–113 MBq) were performed as described previously by Beykan et al. [17] at Aalborg University Hospital, Denmark. A 3D printed kidney phantom for an unbiased assessment was manufactured at the University Hospital Würzburg, Germany.

Animal study

The five Danish Landrace pigs enrolled into our study originated from a specific pathogen-free farm, where all animals were regularly tested for infectious agents (bacteria and viruses). The animals underwent up to 7 days of acclimatization prior to study start. Prior to the study, all animals were confirmed to be in good health. Anesthesia was induced with a Zoletil 50 Vet mixture as described by Beykan et al. [17], and it was maintained with continuous intravenous infusions of

midazolam and fentanyl based on the clinical demand. The levels of pH, CO_2 and potassium were tested in arterial blood samples (ABL 800, Radiometer, Copenhagen, Denmark) [17]. The inspired oxygen fraction was 60%. Several blankets were used to keep the body temperature of the animals under control against hypothermia. The blood pressure and ECG of the animals were monitored continuously using a DatexOhmeda S/5 (GE Healthcare, Broendby, Denmark) [17]. Except pig 5, all pigs received an intravenous amino acid infusion (28.5 g/L Larginine·HCl, 29.3 g/L L-lysine·HCl, 2.7 g/L NaCl) for ~ 4 h (starting ~ 1 h prior to the [^{177}Lu]Lu-OPS201 administration. All procedures involving animals were performed after a written permission from the Danish Animal Experiments Inspectorate no. 2014–15-0201–00102.

The 3D printed pig kidney Phantom:

To investigate the impact of geometric mean based 2D attenuation correction with applied 2D background subtraction on the planar scans and the resulting effect on the TIACs under precisely known conditions, a fillable one-compartment kidney phantom (see Fig. 1) was designed based on the average right kidney dimensions of the five pigs. The right kidney was selected, since there was no visually observable organ-count overlay on the respective whole-body planar scans, keeping the influence of organ-count overlay on the results of this work as low as possible. The 3D printed phantom was modeled as an ellipsoid (Fig. 1) based on the semi-axes lengths of drawn right kidney volumes of interests (VOIs) on the reconstructed pig CT scans performed in syngo.via (Siemens Healthineers). To obtain the dimensions of the ellipsoid, the length, width, and height of each pig's right kidney were measured. The resulting mean semi-axes were 9.73 cm, 5.10 cm, and 2.45 cm, leading to a nominal volume of 63 cm^3. The model was implemented as computer-aided design in Inventor (Autodesk Inc), exported in the stereolithography format, and 3D printed with a Form 2 3D printer using Clear V4 photopolymer resin (Formlabs Inc). After printing, the phantom was refined by washing in isopropyl alcohol, ultraviolet curing, removal of support material, thread cutting, and the addition of screws and o-rings (for filling and mounting).

The phantom experiment was performed as follows: First, the insert was filled with 3.6 MBq of ^{177}Lu (activity concentration: 57.1 ± 0.75 kBq/ml) and placed in a water filled NEMA IEC PET body phantom. To ensure a stable solution, ^{177}Lu chloride was dissolved in 0.1 M HCl with 100 ppm of stable lutetium [27]. Subsequently, a background activity concentration of 5.72 ± 0.11 kBq/ml was injected in the NEMA IEC PET body phantom.

The activity concentration ratio between the background and the kidney insert was 9.94. Both activity concentrations were obtained based on three 1-mL aliquots of each of the two stock solutions, which were subsequently measured in a calibrated high-purity Germanium detector. All activities were decay-corrected to the starting time of the respective acquisitions.

Image acquisition and reconstruction of the pig and phantom data

Multiple time-point whole-body planar and SPECT/CT scans of the pigs were performed on a Siemens Symbia T16 (Crystal Thickness: 9.5 mm) at Aalborg University Hospital, Denmark. The individual scan-tps of each pig PI can be seen in the Supplementary file's Table 1. For each pig, at each scan-tp PI, a 10-min whole-body planar scan was performed with a scan velocity of 1.67 mm/s, and a 40-min whole-body SPECT scan was performed (2 bed positions, 20 min per bed position). The scans of the pigs were reconstructed at University Hospital Würzburg, Germany.

The phantom preparation as well as the SPECT/CT and planar scans of the phantom including the reconstructions were performed at the University Hospital Würzburg, Germany on a Siemens Intevo Bold SPECT/CT system (Crystal Thickness: 9.5 mm). Several sequential phantom measurements were performed to mimic the biokinetics in the right kidney of pig 1. In other words, a phantom measurement had to be performed for each of the seven scan-tps PI (and equivalently each determined right kidney activity), at which pig 1 had been imaged. The most straightforward option would have been to fill the phantom multiple times. Due to some disadvantages, which will be explained in more detail in the discussion section, instead of changing the amount of activity in the kidney phantom and leaving the acquisition duration unchanged, we decided to use a single phantom activity and change the acquisition duration to mimic the different count values observed in the measurements of pig 1. This approach offers the advantages that it only required a single phantom preparation, and that the entire series of measurements could be completed in a few hours. All acquisition durations (whole-body planar and SPECT/CT scans) are shown in Table 1. For the scan-tp at 54 h PI, for which the highest total number of counts in the right kidney of pig 1 was observed, the scan duration was set to 20 min (same as a single bed position in pig 1 SPECT measurements). Subsequently, the scan duration of all other measurements was adjusted to mimic the count numbers resulting from all other (lower) activities. Pig 1 was selected as model for our phantom experiments as more scan-tps PI were available for pig 1 than for any other pig (see the Supplementary file's Table 1).

Subsequent to the SPECT acquisitions of the phantom and the pigs, a low-dose CT scan was acquired for attenuation correction (see Table 2). In addition to the attenuation correction, a triple-energy window based scatter correction was applied for each 3D scan of the phantom and the pigs (see Table 2). The reconstructions were performed by using Flash3D iterative reconstruction algorithm, 6 iterations and 6 subsets with a 6 mm Gaussian filter. Further SPECT acquisition settings and

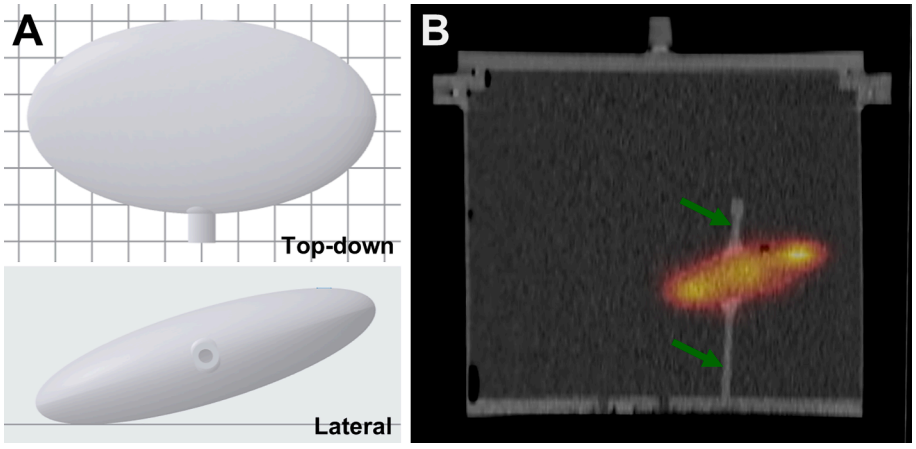

Fig. 1. 3D printed pig kidney phantom. Left, A: STL-File in the slicing software PreForm (Formlabs Inc) from top-down and lateral perspective. Right, B: SPECT/CT image of the 3D printed pig kidney phantom filled with ^{177}Lu in syngo.via (Siemens Healthineers). [The attachment and filling ports (green arrows) were separately designed, modeled, and agglutinated after the 3D printing process.]. (For interpretation of the references to color in this figure legend, the reader is referred to the web version of this article.)

Table 1
Total acquisition durations for each performed whole-body planar and SPECT/CT scan of the phantom corresponding to each scan-tp of pig 1 PI.

Pig 1 SPECT/CT scan-tps PI (h)	Total acquisition duration for the SPECT/CT scan of the phantom (min)
0.7	14.4
1.9	18.1
3.0	19.4
54.0	20.0
101.4	12.8
148.9	8.21
293.7	3.12

Pig 1 whole-body planar scan-tps PI (h)	**Total acquisition duration for the whole-body planar scan of the phantom (min)**
0.3	14.4
1.6	18.1
2.7	19.4
54.4	20.0
102.0	12.8
149.1	8.21
293.8	3.12

Table 2
SPECT/CT acquisition and reconstruction parameters for the pigs and the phantom.

Settings	Pigs	Phantom
Selected Energy window	188–227 keV	188–224 keV
Lower scatter window	165–186 keV	165–186 keV
Upper scatter window	227–248 keV	227–248 keV
Matrix size	128 × 128	128 × 128
Detector motion	step-and-shoot mode	step-and-shoot mode
Number of projections	120	120
Collimator	Medium Energy	Medium Energy
Scan arc	180	180
Number of angular steps	3	3
Number of bed positions	2	1
Detector movement	auto-contour mode	auto-contour mode
CT	low dose CT scan (130 kV with 22 mAs)	low dose CT scan (130 kV with 28 mAs)
Reconstruction	FLASH-3D iterative reconstruction algorithm, 6 iterations and 6 subsets, a 6 mm Gaussian filter	FLASH-3D iterative reconstruction algorithm, 6 iterations and 6 subsets, a 6 mm Gaussian filter
Applied corrections	CT-based attenuation correction and triple-energy-window based scatter correction	CT-based attenuation correction and triple-energy-window based scatter correction

reconstruction details can be seen in Table 2.

The 2D attenuation and 2D background corrections applied to the whole-body planar scans and the count-activity conversions for the 2D and 3D scans are explained in detail in the section 'Activity Quantification and Integration of the TACs'.

The image calibration factors were 18 and 20 counts per seconds per MBq for the Siemens Symbia T16 and the Siemens Intevo SPECT/CT systems, respectively. The calibration for the Siemens Symbia Intevo was performed according to the calibration protocol that was developed during the MRTDosimetry project as described in the paper by Tran-Gia, et al. [28] by using measurement of a Jaszczak cylinder filled with a known activity of ^{177}Lu. For the pigs scanned at Aalborg University Hospital, the whole-body uptake of the first scan was set to 100%, resulting in an image calibration factor of 18 counts per seconds per MBq [17].

Taking into account the low amount of administered ^{177}Lu activities as 97–113 MBq in this study, no dead-time correction method was applied since the dead-time related count-loss can be expected to be negligible for the count rates present [28,29].

Imaging methods used for dosimetry

In total, three different imaging approaches were used for dosimetry: multiple time-point SPECT/CT imaging (used for imaging-protocol A), multiple time-point planar scans in combination with one SPECT/CT imaging (used for imaging-protocol B) and single time-point SPECT/CT imaging (imaging-protocol C). For the imaging-protocol B, whole-body planar scans at multiple time points in combination with one SPECT/CT scan ~ 3 h PI were used. For the imaging-protocol B, the used SPECT/CT scan-tp PI was determined based on the highest amount of activity accumulated in the right kidney of the pigs.

The highest activity accumulation for 3 out of 5 pigs was found at ~ 3 h PI, whereas for the remaining 2 pigs, the highest activity accumulation was found at ~ 54 h PI. For the two pigs, the relative activity difference between the ~ 3 h and the ~ 54 h SPECT/CT scans PI was<5%. Therefore, the ~ 3 h SPECT/CT scan PI was selected for the imaging-protocol B.

Dosimetry analysis

Activity quantifications and integration of the TACs

Activity quantification and integration of the TACs for each pig and the phantom were performed using the NUKDOS software [30]. NUKDOS enables 3D segmentation as well as 2D segmentation with automatic background count subtraction and geometric mean calculation.

After loading the 2D and 3D scans in the NUKDOS software, an image calibration factor that is specific to the employed SPECT/CT system must be entered. Only after that, the region of interest (ROI) and VOI analysis can be performed.

In addition, NUKDOS provides an assessment of the goodness of the fitting function performed for the TACs as well as the uncertainties of the TIACs.

Prior to the activity quantification and the TAC integration, the required input data of the actual administered activity, the day and the time of the administration as well as the day and the time of the activity measurement must be entered into NUKDOS. In the next step, the 2D and 3D scans are loaded. The time differences between the administration and the performed scans PI were automatically calculated by NUKDOS. After loading the 2D and 3D scans, image c calibration factor specific to the SPECT/CT system used for data collection must be entered, before a region of interest (ROI) and VOI analysis can be performed.

For each pig and the phantom, the imaging-protocol A and B based percentage uptakes of the right kidneys as a function of time were calculated via ROIs and VOIs manually drawn on the multiple time-point whole-body planar and SPECT/CT scans, respectively.

All ROIs and VOIs were drawn by the same medical physicist with seven years of experience in clinical dosimetry. For the 3D uptake quantification, SPECT/CT scans were not co-registered. VOIs were drawn manually on each SPECT/CT scan-tp PI for each pig and the phantom as in NUKDOS, the automatic VOI transfer feature was not applicable. However, the volumes of the drawn VOIs for each scan-tp were similar (relative volume difference: <6%). All VOIs were delineated based on the CT scan. To account for spilled-out counts, the CT based VOIs were enlarged by two SPECT voxels [31].

In the 2D uptake quantification, four ROIs were drawn for each pig and the phantom: a whole-body ROI, a whole-body background ROI, a right kidney ROI and a right kidney background ROI were delineated on the first whole-body planar scan PI (for both the anterior and the posterior view). After delineating the ROIs, the background count

subtraction and the calculation of the geometric mean were performed automatically by NUKDOS [30]. NUKDOS automatically transfers the ROIs to the other whole-body planar scans, which are not co-registered but can be manually adjusted for each time-point. The areas of the ROIs were identical for each scan-tp PI. If the user applies any adjustments on an ROI, NUKDOS automatically corrects the ROI size on the other whole-body planar scans and subtracts the background counts for the anterior and posterior views. By using these data, the geometric mean counts for the ROIs are calculated. With the count information from the drawn VOIs and ROIs, the imaging-protocol A and B based kidney percentage uptakes versus time for each pig and the phantom were calculated. The counts concerning the delineated ROIs and VOIs were automatically converted to percentage uptake values by NUKDOS, which requires the image calibration factors and the amount of administered activity as inputs.

For the uptake values of the phantom, additional normalization was performed with respect to the SPECT/CT based right kidney uptake values of pig 1 at 3 h PI. As a result of the normalization, the best agreement between the biokinetics of the 3D printed phantom and the right kidney of pig 1 was obtained.

After the 3D and 2D uptake quantifications, the imaging-protocol A and B based right kidney TACs for each pig and the phantom were separately integrated, choosing either the optimal fit function or the highly suggested fit function as proposed by NUKDOS, and TIACs and the corresponding uncertainties were calculated. The NUKDOS related fit function parameters are reported separately. The optimal fit function provided by NUKDOS represents the combination of two fit functions, which is used to calculate the corresponding TIAC with respect to their ranking percentage. For the pigs, all of the TIAC calculations were performed using the optimal fit functions.

On the other hand, while performing the head-to-head comparisons between pig 1 and the phantom by using 7, 6 and 5 scan-tps PI, the highly suggested (ranked > 75%) fit function proposed by NUKDOS was used to eliminate any error associated with using different fit functions, which may directly affect the TIAC calculation. In case the ranking of the highly suggested fit function was not higher than 75%, optimal fit functions were used for consistency.

The scan-tps PI used to calculate the imaging-protocol A and B based right kidney TIACs of pig 1 and the 3D printed pig kidney phantom can be seen in the Supplementary file's table 6a.

The relative percentage difference between the imaging-protocol A and B based TIACs as well as TIAC uncertainties were calculated for each pig and the phantom. The influence of the geometric mean based 2D attenuation correction with applied 2D background subtraction on the TIACs was investigated by using pig 1 and the phantom data. Pig 1 data together with the phantom data was also used to show the effect of late scan-tps PI on dosimetry. For that purpose, the imaging-protocol A and B based TACs including 5, 6 and 7 scan-tps PI were analyzed, and the resulting phantom TIACs were compared with the TIACs of pig 1.

Absorbed dose (AD) calculation

IDAC-DOSE 2.1 [32] and the imaging-protocol C-formula [23] were used to calculate the absorbed doses (ADs). For each pig, the AD per administered activity was reported. For IDAC-DOSE 2.1, the calculated TIACs were used as input values to calculate the ADs with respect to the actual CT based organ volumes. The imaging-protocol C based ADs per administered activity were calculated separately for each of the SPECT/CT scan acquired at > 24 h PI.

The imaging-protocol C based simplified dosimetry approach refers to equation (1) [33] where r_S is the tissue under investigation, $D(r_S)$ is the total absorbed dose to r_S by self-irradiation, $A(r_S,t)$ is the accumulated activity in r_S as a function of time after the administration, and $S(r_S \leftarrow r_S)$ is the absorbed dose per decay or the dose rate per unit activity. The beta energy per decay imparted by ^{177}Lu emitted by beta emissions within the organ is almost independent of the size and shape of the organ due to the short range of the electrons [34,35]. In this study, we only perform mean organ-based dosimetry, potential variations of the spatial and temporal activity distribution in the organ are not directly considered. As described in the publication by Hänscheid H., et al. [23], with reference to the sphere model in OLINDA/EXM [36], a constant factor of 0.25 Gy·g/MBq/h, with an uncertainty of 2% for spherical objects with masses from 10 g to 1 kg, is applied to convert the SPECT/CT scan data and the information on the kidney mass to an absorbed dose (equation (2)). Therefore, equation (1) can be approximated by equation (2) with<10% deviation when the ratio between the SPECT/CT scan time PI and the effective half-life of the administered radionuclide is in the range between 0.75 and 2.5 [23]. Step by step simplification details were performed as reported in the publication by Hänscheid H., et al. [23].

$$D(rS) = \int_{t=0}^{\infty} A(r_s.t) \cdot S(r_s \leftarrow r_s) \cdot dt \quad (1)$$

$$D(rS) \approx 0.25 \frac{Gy{\cdot}g}{MBq{\cdot}h} \frac{TC \cdot t}{ADC \cdot Kidney\ Mass \cdot image\ calibration\ Factor} \quad (2)$$

Here, TC (unit: counts) and t (unit: h) represent the total number of counts in the drawn region and the SPECT/CT's scan-tp PI, respectively, whereas ADC (unit: h) represents the total acquisition duration of the SPECT scan post-injection (image calibration factor unit: counts per h per MBq).

Results

The multiple time-point SPECT/CT imaging used for the imaging-protocol A and the multiple time-point whole-body planar scans in combination with one SPECT/CT imaging used for the imaging-protocol B can be seen in Figs. 2 and 3, respectively. Based on both the 2D and the 3D scans of the pigs, the majority of the [^{177}Lu]Lu-OPS accumulation was observed in the spine, the bones and the kidneys. In Fig. 2 and Fig. 3, concerning the 2D and 3D scans of pig 1, the specific biodistribution of [^{177}Lu]Lu-OPS in the bones, the spine and the kidneys The imaging-protocol A and B based right kidney TACs of the pigs including their NUKDOS related fits are shown in Fig. 4 (left: imaging-protocol A, right: imaging-protocol B). Pig specific percentage uptakes versus time can be also seen in the supplementary file's table 2. The resulting imaging-protocol A and B based right kidney TIACs of the pigs are shown in Fig. 5. The corresponding TIAC uncertainties, used fit functions and the percentage ranking of used fit functions are reported in the Supplementary file's table 3. Further information associated with the NUKDOS related fit function parameters can be seen in the Supplementary file's tables 4 and 5. The TACs, which are created for the head-to-head comparison of the phantom and pig 1, are shown in Fig. 6 (left: imaging-protocol A, right: imaging-protocol B). The same tendency of increase (<54 h) and decrease (>54 h) was obtained for the imaging-protocol A and B based phantom TACs as it was observed in the imaging-protocol A based right kidney TACs of pig 1 (triangles in Fig. 6). The percentage uptakes versus time for the phantom and pig 1 can be also seen in the Supplementary file's table 2. The resulting imaging-protocol A and B based right kidney TIACs for pig 1 and the phantom are shown in Table 3. The corresponding TIAC uncertainties, used fit functions and the percentage ranking of used fit functions according to the used different scan-tps PI were also reported in the Table 3. As described in the Methods, the highly suggested fit function by NUKDOS was used for the TIACs calculated based on 7 and 6 scan-tps PI, as they were ranked > 75%. In contrast, the optimal fit function proposed by NUKDOS was used for the 5 scan-tp PI calculation, as the suggested fit function's ranking was < 75% in this case.

The imaging-protocol A and B based right kidney TIACs of pig 1 and the phantom including their TIAC uncertainties, used fit functions and the percentage ranking of used fit functions according to the used

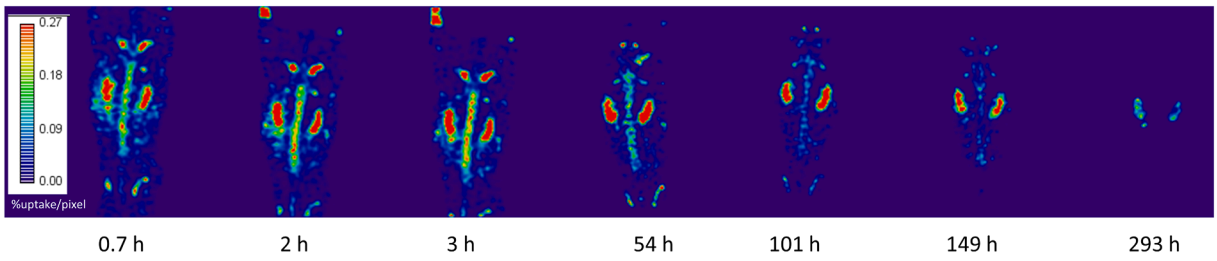

Fig. 2. Coronal views of multiple time-point SPECT/CT scans for pig 1 at 0.7, 2, 3, 54, 101, 149 and 293 h post-injection. [These scans were used for the Imaging-protocol A (multiple time-point SPECT/CT imaging). All SPECT/CT scans were scaled corresponding to the total counts in the first whole-body planar scan at 0.7 h scan post-injection. Color bar represent the percentage uptake value per pixel. For all scans, the major accumulation of [^{177}Lu]Lu-OPS201 was observed in bones, spine and kidneys.].

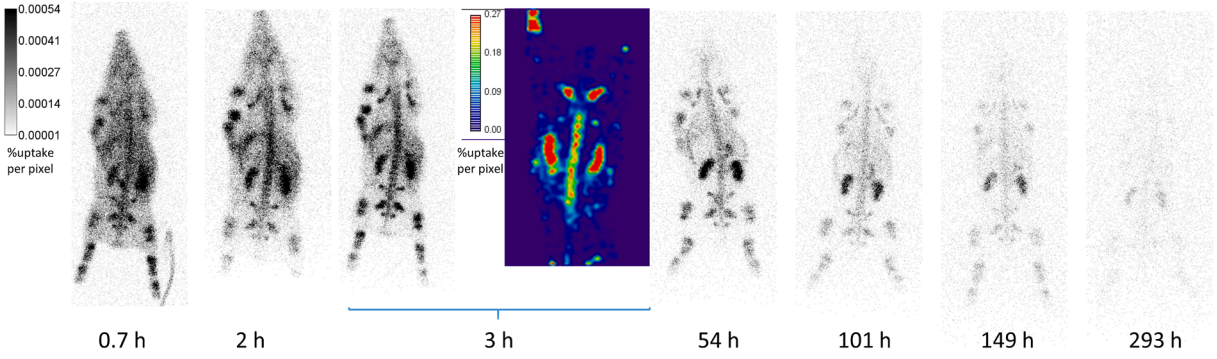

Fig. 3. Coronal views of multiple time-point whole-body planar scans for pig 1 at 0.7, 2, 3, 54, 101, 149, 293 h post-injection in combination with a SPECT/CT scan performed at approximately 3 h post-injection. [These scans were used for the Imaging-protocol B (multiple time-point 2D scans in combination with one SPECT/CT imaging). All planar scans were scaled corresponding to the total counts in the first whole-body planar scan at 0.7 h scan post-injection. Since the highest kidney uptake was observed at ~ 3 h SPECT/CT PI for the majority of the pigs (3/5 pigs), ~3h SPECT/CT PI was used for the the imaging-protocol B. Color bar represent the percentage uptake value per pixel. For all scans, the major accumulation of [^{177}Lu]Lu-OPS201 was observed in bones, spine and kidneys.].

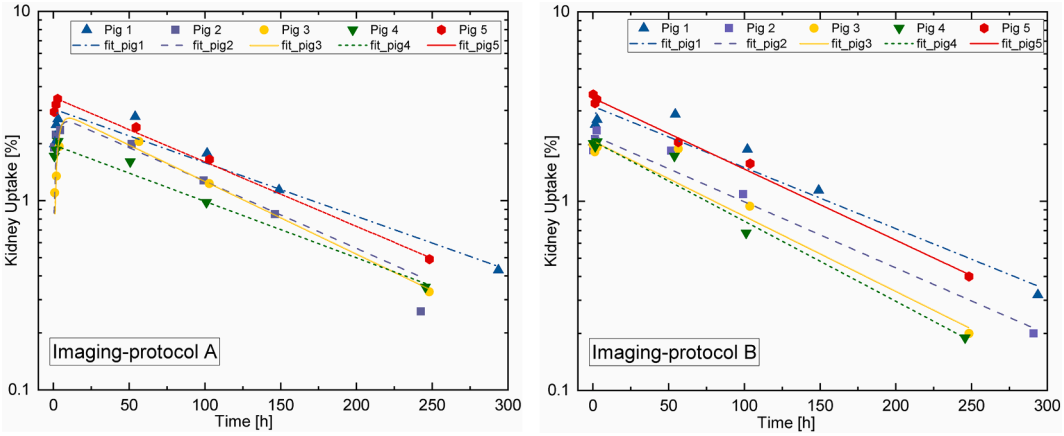

Fig. 4. Imaging-protocol A and B based right kidney time activity curves for the pigs including their NUKDOS related fits. [Imaging-protocol A: Multiple time-point SPECT/CT imaging, Imaging-protocol B: Multiple time-point 2D scans in combination with one SPECT/CT imaging].

different scan time-points PI are summarized in Table 3 (NUKDOS related fit function parameters can be seen in the Supplementary file's tables 6b and 7).

Regarding the TIACs calculated based on TACs including seven scan-tps PI, the imaging-protocol A based TIAC of the phantom was 2.1% higher than the imaging-protocol A based TIAC for pig 1. Similarly, the imaging-protocol B based TIAC of the phantom (including 7 scan-tps PI) was 2.4% higher compared to the imaging-protocol B based TIAC of pig 1 (see Table 3).

For pig 1, the elimination of the last scan-tp PI (294 h PI) from the TACs resulted in TIAC increases of 9% and 26% for the imaging-protocol A and B, respectively, as well as a TIAC uncertainty increase by a factor of 3 (see Table 3). When applying the same elimination to the phantom TACs, a 13% TIAC increase for the imaging-protocol A and a 9% TIAC decrease for the imaging-protocol B were calculated as well as a TIAC uncertainty increase by a factor of 3 and 2 for the imaging-protocol A and B, respectively (see Table 3).

For pig 1 and the phantom, eliminating the last two scan-tps PI (149 h PI and 294 h PI) from the imaging-protocol A based kidney TACs resulted in 1.5 times higher TIACs for both pig 1 and the phantom as well as a TIAC uncertainty increase by a factor of 5 (see Table 3). When the same elimination was performed for the imaging-protocol B based TAC

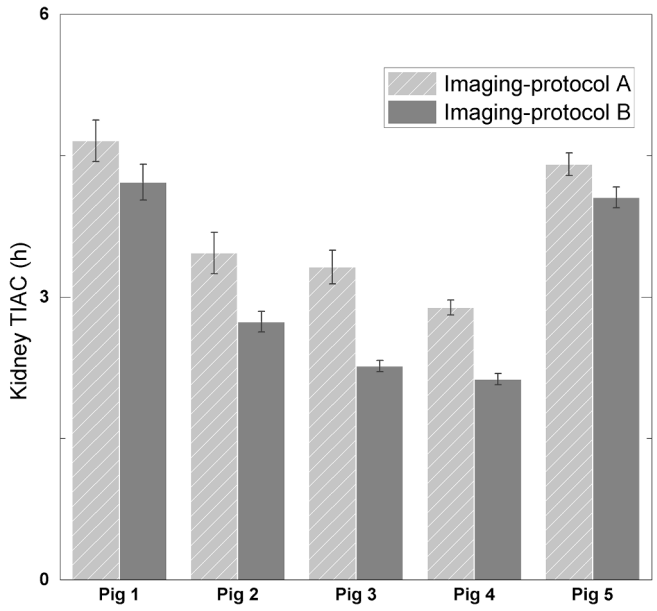

Fig. 5. Imaging-protocol A and B based right kidney TIACs of the pigs including their corresponding TIAC uncertainties. [Imaging-protocol A: Multiple time-point SPECT/CT imaging, Imaging-protocol B: Multiple time-point 2D scans in combination with one SPECT/CT imaging].

of pig 1 and the phantom, a TIAC increase by a factor of 1.5 for the phantom and by a factor of 1.8 for pig 1 was observed. Similarly for the imaging-protocol B, eliminating the 149 h and 296 h scan-tps PI resulted in higher TIAC uncertainties by a factor of 5 for the phantom and by a factor of 7 for pig 1 (see Table 3).

According to the comparison between the imaging-protocol A and B based kidney TIACs (calculated using all scan-tps PI) in each pig, the imaging-protocol B based kidney TIACs were lower than the imaging-protocol A based kidney TIACs for each pig. For pigs 2, 3, and 4, the relative difference between the imaging-protocol A and B based TIACs was in the range from −32% to −21%, whereas it was −10% for the other two pigs (reference: imaging-protocol A based TIACs). A similar underestimation of TIACs in the imaging-protocol B based results compared to the imaging-protocol A based results was observed in the phantom experiments. The imaging-protocol B based TIAC calculated using 7 scan-tps PI was 10% lower than the imaging-protocol A based TIAC of the phantom (see Table 3).

The imaging-protocol A, B and C based ADs per administered activity for the right kidneys of the pigs and the phantom are given in Fig. 7 and in Table 4, respectively. For pigs 3, 4 and 5, since no SPECT/CT scan was performed at ~ 150 h post-injection, the imaging-protocol C based absorbed doses per administered activity were not calculated (see Fig. 7).

For all datasets, the imaging-protocol B based ADs per administered activity were always lower than the imaging-protocol A based ADs per administered activity (see Figs. 7 and 8). Similarly, the imaging-protocol C based ADs per administered activity using the SPECT/CT scan at ~ 50 h and ~ 300 h PI resulted in lower ADs per administered activity compared to the imaging-protocol A based results for both the phantom and the pig datasets (maximum difference regarding the ADs per administered activity: −50%, see Fig. 8). The highest relative difference between the imaging-protocol A and C based ADs per administered activity were calculated by using the ~ 300 h SPECT/CT scan (see Fig. 8). On the other hand, for the phantom and the pig datasets, the imaging-protocol C based ADs per administered activity using SPECT/CT scans at ~ 100 h and ~ 150 h PI were similar to the values obtained by the imaging-protocol A approach (taking the imaging-protocol A based values as reference, the percentage relative difference was > ±5%, see Fig. 8). However, the best agreement was achieved by using ~ 100 h SPECT/CT scan PI. The percentage difference of ADs per administered activity between the imaging-protocol A and the imaging-protocol C at ~ 100 h PI was less than ± 4% for both datasets (see Tables 3 and 4).

Discussion

The ADs per administered activity for the right kidneys of the pigs and the phantom were calculated by using three different imaging

Table 3
Imaging-protocol A and B based right kidney TIACs of pig 1 and the phantom including their corresponding TIAC uncertainties, used fit functions and the percentage ranking of used fit functions according to the used different scan time-points post-injection. [Imaging-protocol A: Multiple time-point SPECT/CT imaging based dosimetry, Imaging-protocol B: Multiple time-point 2D scans in combination with one SPECT/CT imaging based dosimetry. The used fit functions were abbreviated as 3 and 4. Their full equations can be seen at the bottom of the table.].

Right kidney TIACs ± Uncertainty (h) [NUKDOS fit function including their usage percentage]			
Imaging-protocol	Scan time points	Phantom TIAC ± Uncertainty (h)	Pig 1 TIAC ± Uncertainty (h)
A	7	4.8 ± 0.2 [4(100%)]	4.7 ± 0.2 [4(100%)]
	6	5.4 ± 0.6 [4(100%)]	5.1 ± 0.5 [4(100%)]
	5	7.0 ± 1.0 [3(70%), 4 (30%)]	7.1 ± 1.0 [3(67%), 4 (33%)]
Imaging-protocol	Used time points	Phantom TIAC ± Uncertainty (h)	Pig 1 TIAC ± Uncertainty (h)
B	7	4.3 ± 0.2 [4(100%)]	4.2 ± 0.2 [4(100%)]
	6	3.9 ± 0.3 [4(100%)]	5.3 ± 0.6 [4(100%)]
	5	6.6 ± 1.0 [3(53%), 4 (46%)]	7.7 ± 1.3 [3(75%), 4 (25%)]
Fit Function 3:		$A_1 \bullet e^{-(\lambda_1+\lambda_{phys})*t} + A_2 \bullet e^{-(\lambda_{phys})*t}$	
Fit Function 4:		$A_1 \bullet e^{-(\lambda_1+\lambda_{phys})*t} - A_1 \bullet e^{-(\lambda_2+\lambda_{phys})*t}$	

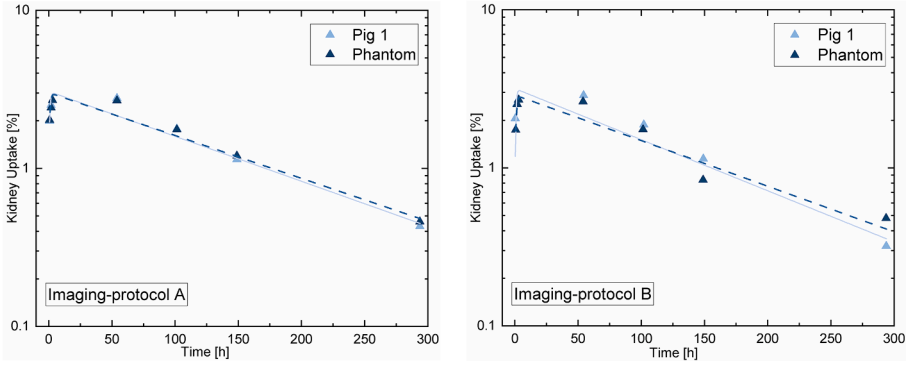

Fig. 6. Imaging-protocol A and B based right kidney time activity curves for pig 1 and the phantom including their NUKDOS related fits. [Triangles represent the percentage uptakes in each scan time-point post-injection. Lines represent the NUKDOS based fits, which were used to calculate the corresponding time-integrated activity coefficients. Imaging-protocol A: Multiple time-point SPECT/CT imaging, Imaging-protocol B: Multiple time-point 2D scans in combination with one SPECT/CT imaging].

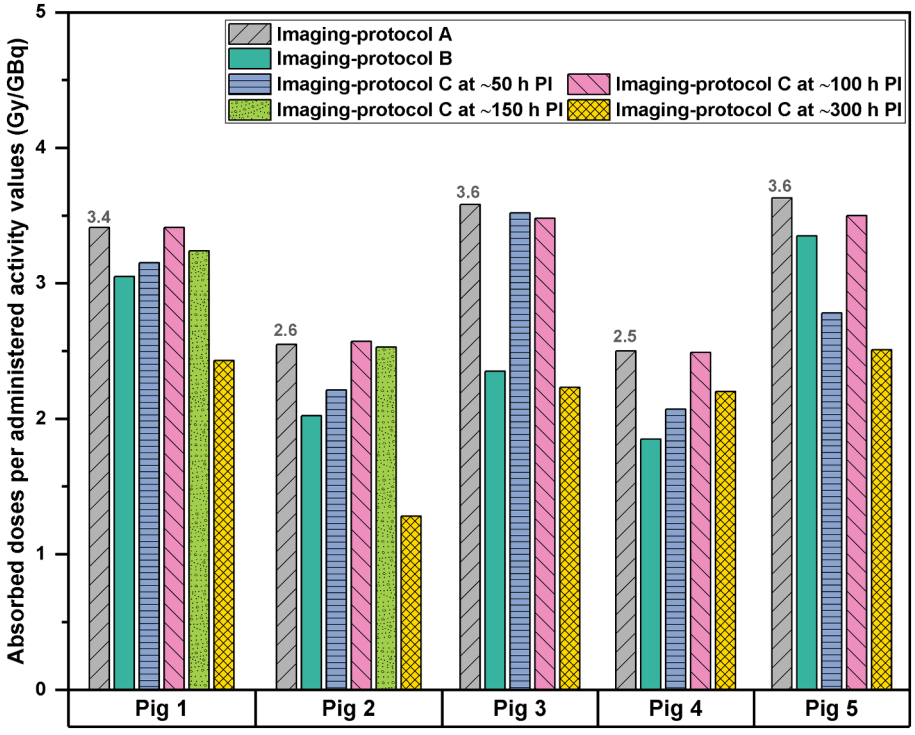

Fig. 7. Absorbed doses per administered activity for the right kidneys of the pigs illustrating the different imaging protocols, the imaging-protocol A based absorbed doses per administered activity (denoted in grey) are taken as reference value. [Imaging-protocol A: Multiple time-point SPECT/CT imaging, Imaging-protocol B: Multiple time-point 2D scans in combination with one SPECT/CT imaging, Imaging-protocol C: Single time-point SPECT/CT imaging, AD: Absorbed dose, PI: Post-injection. The imaging-protocol A based absorbed doses per administered activity were considered as reference values. As for pigs 3, 4, and 5 no SPECT/CT scan at 150 h PI was performed, the imaging-protocol C based absorbed doses per administered activity are not shown.].

Table 4
Imaging-protocol A, B and C based ADs per administered activity of the phantom. [Imaging-protocol A: Multiple time-point SPECT/CT imaging based dosimetry, Imaging-protocol B: Multiple time-point 2D scans in combination with one SPECT/CT imaging based dosimetry, Imaging-protocol C: Single time-point SPECT/CT imaging based dosimetry, AD: Absorbed dose.].

Imaging-protocol	Imaging-protocol A, B and C based ADs per administered activity (Gy/GBq)
A	6.630
B	5.790
C including 54 h PI SPECT/CT scan	5.605
C including 101 h PI SPECT/CT scan	6.858
C including 149 h PI SPECT/CT scan	6.907
C including 294 h PI SPECT/CT scan	5.155

protocols for dosimetry (imaging-protocol A, B and C). To find if there are accurate alternatives to imaging-protocol A based ^{177}Lu kidney dosimetry, the imaging-protocol B and C based TIACs and ADs per administered activity were compared to the imaging-protocol A based results.

The right kidney of the pigs was selected for the investigations since there was no visible 2D organ-count overlays (counts from above or below the kidney overlayed with the kidney in the 2D projection). This way the influence of 2D organ-count overlays on dosimetry was reduced.

The ideal SPECT/CT scan-tp PI for the imaging-protocol B was determined based on the highest amount of activity accumulated in the right kidney of the pigs. The highest activity in the right kidneys was found for the ~ 3 h SPECT/CT scan PI (for 3 out of 5 pigs) and for the ~ 54 h SPECT/CT scan PI (for 2 out of 5 pigs). For the two pigs, the relative accumulated activity difference between ~ 3 h and ~ 54 h SPECT/CT scans PI was only 5%. Therefore, the ~ 3 h SPECT/CT scan PI was used for the imaging-protocol B.

The choice not to perform several sequential phantom experiments to mimic the right kidney activities of the pig 1 measurements was based on the following considerations: 1) a different stock solution would have been necessary for each kidney activity, which directly increases the uncertainties associated with the preparation. 2) Emptying the phantom after each measurement could have caused problems with stock solution remaining at the inner phantom walls or, alternatively, led to long times between consecutive measurements. In addition, multiple fillings and emptyings would have been problematic regarding radiation protection. An alternative could have been to fill the phantom with the highest activity concentration measured in the right kidney of pig 1 and to perform imaging at multiple time-points during the decay, closely matching the activities measured for the right kidney of pig 1. This, however, would have introduced potential errors in the homogeneity of the stock solution inside the kidney as the last measurement would have been performed two weeks after preparing the phantom.

The main limitations of our study were i) the small number of pigs which results from animal handling procedures and expenses and ii) the lack of ~ 24 h SPECT/CT scans PI which is related to the regulations of the anesthesia injection. However, since the relative activity difference between ~ 3 h and ~ 54 h SPECT/CT scans PI was<5% in each pig, the influence of the missing ~ 24 h SPECT/CT scans PI on the TIACs and ADs is considered to be low. Also, due to limitations in the animal handling procedures, we could not enroll more pigs. As the [^{177}Lu]Lu-OPS201 biodistribution was similar in the right kidneys of the five pigs, however, we believe that the results of five pigs, which were reported here, is sufficient to represent the ground truth of our analysis on the image-based kidney dosimetry in dependence of the used different imaging protocols.

Of course, preclinical studies including a higher number of pigs as well as clinical studies with more than five patients would be desirable. They are, however, not easy to implement due to financial and ethical constraints.

Another limitation is the lack of patient data. In clinical routine, it is very demanding to acquire whole-body planar and/or SPECT/CT scans for multiple time-points (e.g., more than five times), especially for late time-points (e.g., >150 h PI). However, in our previous study, it was shown that the kidney biokinetics of [^{177}Lu]Lu-OPS injected pigs and patients were comparable despite the observed interspecies differences

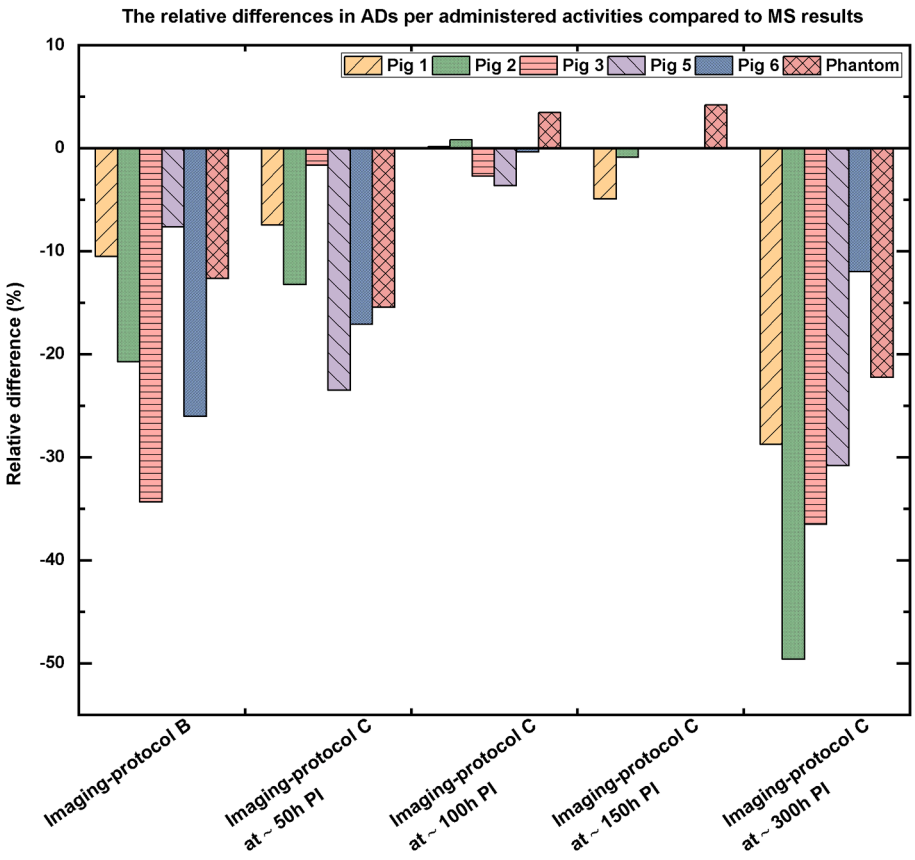

Fig. 8. The percentage relative differences in Imaging-protocol B and C based ADs per administered activity compared to the imaging-protocol A based ADs per administered activity. [Imaging-protocol A: Multiple time-point SPECT/CT imaging, Imaging-protocol B: Multiple time-point 2D scans in combination with one SPECT/CT imaging, Imaging-protocol C: Single time-point SPECT/CT imaging, PI: post-injection, AD: Absorbed dose. The scan time-points for each pig are similar but not identical, therefore, the symbol '~' is used].

concerning spleen and spine [18]. As the pigs underwent scans at more time-points than the patients, we preferred to use the pigs' kidney data for the investigations performed in this study.

The use of different SPECT/CT systems for the measurements of the pigs and the phantom might introduce uncertainties in the activity determination, which may be associated with the site-specific calibration of the radionuclide calibrators and the filling procedure of the phantom, which is used for calibration. However, a recently published comparison exercise by the MRTDosimetry collaboration [28] showed a very high degree of harmonization of quantitative SPECT/CT imaging across multiple sites if the same setup (i.e., combination of detector, acquisition, and reconstruction) is used [28]. As the same detector, acquisition and reconstruction were used in our study at both sites in Denmark and Germany, the related uncertainties can be assumed to be low.

For the dosimetry analysis, although the possibility of evaluating the late scan-tps PI was essential, the impact of SPECT activity quantification accuracy for low count statistics (e.g., at late scan-tps PI) might affect the analysis. In our study, SPECT acquisitions of the phantom at 54 h and 294 h PI were used to assess the impact of SPECT activity quantification accuracy of low count statistics at late scan-tps PI (highest kidney uptake: 54 h PI, lowest kidney uptake: 294 h PI). Measured counts in the kidney compartment of the phantom mimicking the SPECT acquisitions at 54 h and 294 h PI were compared to the calculated counts (derived using the image calibration factor and the injected amount of activity) at corresponding scan-tps PI. The measured count numbers were lower than the calculated count numbers for all scan-tps PI (32.5% for 54 h and 13.0% for 294 h with a mean of 27.7%±7.0%). Therefore, the impact of low count statistics, as they could occur for late scan-tps PI, is negligible with respect to the results of our study.

For the imaging-protocol B, organ-count overlays on whole-body planar scans are listed in the literature as a main reason for potential over- or underestimations in AD calculations [24]. In our study, despite the minimization of organ-count overlays (we analyzed only right kidneys since there was no visible 2D organ-count overlays), ADs per administered activity were still underestimated using the imaging-protocol B compared to the imaging-protocol A based results.

For both the pig and the phantom datasets, the imaging-protocol B based kidney uptakes as well as their TIACs and ADs per administered activity were lower than the imaging-protocol A based results. The relative difference between the imaging-protocol A and B based ADs per administered activity for the pigs lay between − 34% and − 8%, whereas it was − 13% for the phantom. This can be explained as follows:

1) The lack of an accurate attenuation correction method for the whole-body planar images. The attenuation on the whole-body planar scans of the pigs and the phantom was only corrected by taking the geometric mean, which will still result in an underestimation of counts in comparison to the SPECT/CT images (where the much more accurate CT based attenuation correction can be applied).
2) The applied background subtraction for the whole-body planar scans (specifically for the phantom data). The conventional subtraction of the background counts from the counts in the kidney insert does not consider the portion of the background equivalent to the volume of the kidney insert. Therefore, a background subtraction may underestimate the kidney activity [24].
3) The inhomogeneous and time-varying background contribution in both the whole-body planar and the SPECT/CT scans (only concerning the pig data), especially regarding the presence of overlapping organs or tissues for the pigs. The calculated higher difference between the imaging-protocol A and B based ADs per administered activity for pigs 3 and 4 (>20%) compared to the other pigs might be mainly related to this effect. Depending on the degree of the inhomogeneous background contributions and their change in time, the ADs might be over- or underestimated.

In contrast to our findings (reference: imaging-protocol A, relative difference between the imaging-protocol A and B based kidney ADs per administered activity: from − 34% to − 8%), Rosar et al. [37] reported that the imaging-protocol B is nearly equivalent to the imaging-protocol A (reference: imaging-protocol A, median difference between the imaging-protocol A and B based kidney ADs per administered activity: −4%). In this study [37], a dosimetry comparison was performed by applying 2D whole-body planar based, imaging-protocol A and B based dosimetry for patients undergoing [^{177}Lu]Lu-PSMA-617 radioligand therapy by using three scan-tps PI (24 h, 48 h and ≥ 96 h PI). The TIACs of the kidneys were calculated based on trapezoidal integration with an assumption of constant activity between the scan-tps at 0 h and 24 h PI. After the last scan-tp PI, a mono-exponential integration was performed considering only physical decay. In addition to the study by Rosar et al. [37], in the study by Belli et al. [22], the imaging-protocol A and B based kidney results including four scan time-points PI (~0.5 h, ~24 h, ~40 h and ~ 90 h PI) were compared for one patient undergoing [^{177}Lu]Lu-PSMA-617 radioligand therapy. The TIACs of the kidneys were calculated using Hermes Internal Radiation Dosimetry Software, applying a tri-exponential fit function. The calculated ADs per administered activity based on the imaging-protocol B were reported to be 1.6% lower compared to the imaging-protocol A based values [22]. The differences between our study and the studies by Rosar et al. [37] and Belli et al. [22] are mainly associated with the performed methodologies for TIAC calculations and the number of scans PI. In addition, while comparing these three studies, it must be taken into account that the type of radioligand or peptide might also affect the comparison between their results and our results. The differences observed between our study and the study by Rosar et al. [37] might be mainly associated with the way of TIAC calculation and their lack of early (≤24 h) and late (≥100 h) scan-tps PI.

Concerning the study by Belli et al. [22], the observed differences might be related to the use of a tri-exponential fit function in the TIAC calculation and the lack of scan-tps PI after 90 h (similar to the study by Rosar et al. [37]).

According to the comparisons between the imaging-protocol A, B and C based ADs of the pigs and the phantom, the imaging-protocol C at ~ 100 h PI showed the best agreement with the imaging-protocol A for both datasets. The maximum relative difference in ADs per administered activity between the imaging-protocol C at ~ 100 h PI SPECT/CT scan and the imaging-protocol A was only − 4% for the pigs and + 3% for the phantom, whereas the maximum relative difference in ADs per administered activity between the imaging-protocol A and B was − 34% for the pigs and − 13% for the phantom. This shows that in the ^{177}Lu somatostatin receptor studies focusing on kidney dosimetry, using one quantitative SPECT/CT scan at ~ 100 h PI might be a better alternative for the time-consuming the imaging-protocol A than the imaging-protocol B. However, one must be aware that the imaging-protocol C requires not only the optimal scan time-point PI and an image quantification with a low uncertainty, but also sufficient knowledge about the biokinetics, which depends on many factors such as the radiopharmaceutical, examined organ, as well as the species under investigation.

In our study, we only focused on kidney dosimetry for the somatostatin receptor antagonist OPS labelled with ^{177}Lu. However, in the study by Hänscheid et al. [23], dosimetry analysis based on multiple time-point whole-body planar images showed that the scan-tp at ~ 96 h PI was optimal for the imaging-protocol C based dosimetry not only for the kidneys, but also for the other organs such as spleen. Considering the results of the study by Hänscheid et al. [23], further studies including a head-to-head comparison between the imaging-protocol A, B and C with multiple organs analyzed are essential.

Another important topic concerning the imaging-protocol C at ~ 100 h PI is the additional effort for the patients. Returning to the hospital at ~ 100 h PI might not be possible for all patients. On the other hand, having only one late SPECT/CT scan at ~ 100 h PI for dosimetry is less demanding and more comfortable for the patients when compared with the alternative of performing multiple time-point SPECT/CT scans at earlier time-points PI.

The observed large differences in ADs by using the SPECT/CT scans at ~ 50 h and ~ 300 h PI for the imaging-protocol C showed the importance of the proper scan-tp selection PI. In the publication by Hänscheid et al. [23], a<10% deviation between multiple and single time-point approaches was found when the ratio between SPECT/CT scan time and effective half-life was in the range of 0.75 and 2.5. In our study, the ratio was only in the defined range for the SPECT/CT scan-tps of ~ 100 h and ~ 150 h PI (see Supplementary file's table 8). For other SPECT/CT scan-tps PI, the ratio was not in the defined range, which explains the high observed differences compared to the imaging-protocol A approach.

Similarly as in imaging-protocol C, the adequate choice of scan-tps PI also plays a considerable role for AD calculations for both imaging-protocol A and B. To investigate the effect of late scan-tps PI (>100 h PI) on ^{177}Lu kidney dosimetry, a phantom study mimicking the imaging-protocol A based uptake of pig 1 was designed. The consistency of the kidney uptake in each SPECT/CT and whole-body planar scan between the phantom and pig 1 datasets showed that, with the chosen count rates and applied normalization, mimicking actual biokinetics of pig 1 was achieved (mean difference: 3%). Mainly due to the three effects mentioned above, the imaging-protocol B based TIACs (using all scan-tps PI) were 10% lower than the imaging-protocol A based TIACs for both datasets.

When the late scan-tps PI were eliminated, as a result of missing information, the selected fit parameters did not represent the actual biodistribution. Therefore, an increase in the imaging-protocol A and B based TIACs and their corresponding TIAC uncertainties was observed up to a factor of 2 and 5, respectively, for both datasets. The two-fold increase in TIAC proportionally affects the ADs and results in an overestimations of the ADs per administered activity.

Conclusion

Based on the 3D printed phantom and the pig studies, we were able to show that in ^{177}Lu somatostatin receptor studies focusing on kidney dosimetry by using multiple time-point SPECT/CT acquisitions, an imaging time point at ≥ 100 h post-injection is essential for an accurate absorbed dose calculation.

Although multiple time-point SPECT/CT images are considered the gold standard in dosimetry, it is time-consuming and, therefore, difficult to integrate into the clinical routine, let alone to have the costs covered by insurances. The most common alternative is a imaging-protocol B approach, which showed large differences (associated with the lack of accurate 2D attenuation correction and 2D background subtraction), although 2D organ-count overlays were minimized in our study setup. Possible differences between the multiple time-point SPECT/CT and the imaging-protocol B based time-integrated activity coefficients as well as absorbed doses of the kidneys in clinical studies related to ^{177}Lu-labelled somatostatin receptor therapies might be higher compared to our study results as, in a clinical studies, the overlapping counts in the abdominal region of the patients might increase the uncertainty of the results in comparison to our study. To sum up, performing imaging-protocol B based dosimetry might result in an unreliable kidney dosimetry due to the underestimated kidney absorbed doses, potentially resulting in kidney toxicity.

On the other hand, the single time-point SPECT/CT approach with only a single SPECT/CT acquired ~ 100 h PI resulted in similar absorbed doses per administered activity (maximum difference < 4%) compared to the multiple time-point SPECT/CT results. Therefore, instead of using the imaging-protocol B, we conclude that using a single SPECT/CT acquired at ~ 100 h PI represents a more accurate, practical, and easy way of performing dosimetry and, therefore, a well-suited alternative for the multiple time-point-SPECT/CT approach. In addition, regarding the cost, a single SPECT/CT image might be more likely to be covered by

insurances than multiple time-point SPECT/CT imaging. Nevertheless, it is important to point out that our preclinical findings (based on five pig measurements and phantom data) are based on [^{177}Lu]Lu-OPS201 kidney dosimetry. Single time-point SPECT/CT dosimetry requires sufficient knowledge about the biokinetics and, therefore, it requires the optimal scan time-points post-injection, which depends on many factors such as the radiopharmaceutical, examined organ, as well as the species under investigation.

Declaration:

Ethical approval:

The animal data used in this study were obtained and retrospectively analyzed from previously published data, for which all ethical approvals were provided in the respective publications [17,18]. All procedures involving pigs were performed after a written permission from the Danish Animal Experiments Inspectorate no. 2014–15-0201–00102 [17].

Consent for publication

Not applicable.

Availability of data and material

The datasets generated during and analyzed during the current study are available from the corresponding author on reasonable request.

Funding

The original pig study was funded by a grant from OctreoPharm Sciences GmbH. Michael Lassmann received a research grant by Octreopharm Sciences GmbH, Ipsen Group.

Authors' contributions

SB, ML, JT-G and SBJ contributed in the conception and design. SB, ML and JT-G contributed in the development of the methodology. SB, ML and JT-G participated in the acquisition of the data. SB, ML and JT-G participated in the analysis and interpretation of the data. All authors participated in the writing and review and/or revision of the manuscript. All authors read and approved the final manuscript.

Declaration of Competing Interest

The authors declare that they have no known competing financial interests or personal relationships that could have appeared to influence the work reported in this paper.

Appendix A. Supplementary data

Supplementary data to this article can be found online at https://doi.org/10.1016/j.ejmp.2022.06.002.

References

[1] Del Prete M, Buteau F-A, Arsenault F, Saighi N, Bouchard L-O, Beaulieu A, et al. Personalized ^{177}Lu-octreotate peptide receptor radionuclide therapy of neuroendocrine tumours: initial results from the P-PRRT trial. Eur J Nucl Med Mol Imaging 2019;46(3):728–42.

[2] Chiesa C, Sjogreen Gleisner K, Flux G, Gear J, Walrand S, Bacher K, et al. The conflict between treatment optimization and registration of radiopharmaceuticals with fixed activity posology in oncological nuclear medicine therapy. Eur J Nucl Med Mol Imaging 2017;44(11):1783–6.

[3] Flux GD, Sjogreen Gleisner K, Chiesa C, Lassmann M, Chouin N, Gear J, et al. From fixed activities to personalized treatments in radionuclide therapy: lost in translation? Eur J Nucl Med Mol Imaging 2018;45(1):152–4.

[4] Bodei L, Cremonesi M, Ferrari M, Pacifici M, Grana CM, Bartolomei M, et al. Long-term evaluation of renal toxicity after peptide receptor radionuclide therapy with 90Y-DOTATOC and 177Lu-DOTATATE: the role of associated risk factors. Eur J Nucl Med Mol Imaging 2008;35(10):1847–56.

[5] Garske-Román U, Sandström M, Fröss Baron K, Lundin L, Hellman P, Welin S, et al. Prospective observational study of ^{177}Lu-DOTA-octreotate therapy in 200 patients with advanced metastasized neuroendocrine tumours (NETs): feasibility and impact of a dosimetry-guided study protocol on outcome and toxicity. Eur J Nucl Med Mol Imaging 2018;45(6):970–88.

[6] Huizing DMV, de Wit-van der Veen BJ, Verheij M, Stokkel MPM. Dosimetry methods and clinical applications in peptide receptor radionuclide therapy for neuroendocrine tumours: a literature review. EJNMMI research 2018;8(1).

[7] Menda Y, Madsen MT, O'Dorisio TM, Sunderland JJ, Watkins GL, Dillon JS, et al. (90)Y-DOTATOC dosimetry-based personalized peptide receptor radionuclide therapy. J Nucl Med 2018;59(11):1692–8.

[8] Sundlöv A, Sjögreen-Gleisner K, Svensson J, Ljungberg M, Olsson T, Bernhardt P, et al. Individualised (177)Lu-DOTATATE treatment of neuroendocrine tumours based on kidney dosimetry. Eur J Nucl Med Mol Imaging 2017;44(9):1480–9.

[9] Chicheportiche A, Grozinsky-Glasberg S, Gross DJ, Krausz Y, Salmon A, Meirovitz A, et al. Predictive power of the post-treatment scans after the initial or first two courses of [(177)Lu]-DOTA-TATE. EJNMMI Phys 2018;5(1).

[10] Zaknun JJ, Bodei L, Mueller-Brand J, Pavel ME, Baum RP, Hörsch D, et al. The joint IAEA, EANM, and SNMMI practical guidance on peptide receptor radionuclide therapy (PRRNT) in neuroendocrine tumours. Eur J Nucl Med Mol Imaging 2013;40(5):800–16.

[11] Bodei L, Cremonesi M, Grana CM, Fazio N, Iodice S, Baio SM, et al. Peptide receptor radionuclide therapy with ^{177}Lu-DOTATATE: the IEO phase I-II study. Eur J Nucl Med Mol Imaging 2011;38(12):2125–35.

[12] Wild D, Fani M, Behe M, Brink I, Rivier JEF, Reubi JC, et al. First clinical evidence that imaging with somatostatin receptor antagonists is feasible. J Nucl Med 2011;52(9):1412–7.

[13] Ilan E, Sandström M, Wassberg C, Sundin A, Garske–Román U, Eriksson B, et al. Dose response of pancreatic neuroendocrine tumors treated with peptide receptor radionuclide therapy using 177Lu-DOTATATE. J Nucl Med 2015;56(2):177–82.

[14] Walrand S, Jamar F. Renal and red marrow dosimetry in peptide receptor radionuclide therapy: 20 years of history and ahead. Int J Mol Sci 2021;22.

[15] European Society of R. Summary of the European Directive 2013/59/Euratom: essentials for health professionals in radiology. Insights Imaging. 2015;6:411-7.

[16] Konijnenberg M, Herrmann K, Kobe C, Verburg F, Hindorf C, Hustinx R, et al. EANM position paper on article 56 of the Council Directive 2013/59/Euratom (basic safety standards) for nuclear medicine therapy. Eur J Nucl Med Mol Imaging 2021;48(1):67–72.

[17] Beykan S, Dam JS, Eberlein U, Kaufmann J, Kjærgaard B, Jødal L, et al. ^{177}Lu-OPS201 targeting somatostatin receptors: in vivo biodistribution and dosimetry in a pig model. EJNMMI Res 2016;6(1).

[18] Beykan S, Fani M, Jensen SB, Nicolas G, Wild D, Kaufmann J, et al. In vivo biokinetics of ^{177}Lu-OPS201 in mice and pigs as a model for predicting human dosimetry. Contrast Media Mol Imaging 2019;2019:1–7.

[19] Wild D, Fani M, Fischer R, Del Pozzo L, Kaul F, Krebs S, et al. Comparison of somatostatin receptor agonist and antagonist for peptide receptor radionuclide therapy: a pilot study. J Nucl Med 2014;55(8):1248–52.

[20] Emami B, Lyman J, Brown A, Cola L, Goitein M, Munzenrider JE, et al. Tolerance of normal tissue to therapeutic irradiation. Int J Radiat Oncol Biol Phys 1991;21(1):109–22.

[21] Rinscheid A, Kletting P, Eiber M, Beer AJ, Glatting G. Technical Note: optimal sampling schedules for kidney dosimetry based on the hybrid planar/SPECT method in ^{177}Lu-PSMA therapy. Med Phys 2019;46(12):5861–6.

[22] Belli ML, Mezzenga E, Di Iorio V, Celli M, Caroli P, Canali E, et al. A whole body dosimetry protocol for peptide-receptor radionuclide therapy (PRRT): 2D planar image and hybrid 2D+3D SPECT/CT image methods. J Vis Exp 2020;(158).

[23] Hänscheid H, Lapa C, Buck AK, Lassmann M, Werner RA. Dose mapping after endoradiotherapy with ^{177}Lu-DOTATATE/DOTATOC by a single measurement after 4 days. J Nucl Med 2018;59(1):75–81.

[24] Siegel JA, Thomas SR, Stubbs JB, Stabin MG, Hays MT, Koral KF, et al. MIRD pamphlet no. 16: techniques for quantitative radiopharmaceutical biodistribution data acquisition and analysis for use in human radiation dose estimates. J Nucl Med 1999;40:37S–61S.

[25] Zimmerman BE, Grošev D, Buvat I, Coca Pérez MA, Frey EC, Green A, et al. Multi-centre evaluation of accuracy and reproducibility of planar and SPECT image quantification: An IAEA phantom study. Z Med Phys 2017;27(2):98–112.

[26] Rinscheid A, Lee J, Kletting P, Beer AJ, Glatting G. A simulation-based method to determine optimal sampling schedules for dosimetry in radioligand therapy. Z Med Phys 2019;29(4):314–25.

[27] Tran-Gia J, Salas-Ramirez M, Lassmann M. What you see is not what you get: on the accuracy of voxel-based dosimetry in molecular radiotherapy. J Nucl Med 2020;61(8):1178–86.

[28] Tran-Gia J, Denis-Bacelar AM, Ferreira KM, Robinson AP, Calvert N, Fenwick AJ, et al. A multicentre and multi-national evaluation of the accuracy of quantitative Lu-177 SPECT/CT imaging performed within the MRTDosimetry project. EJNMMI Phys 2021;8(1).

[29] Frezza A, Desport C, Uribe C, Zhao W, Celler A, Després P, et al. Comprehensive SPECT/CT system characterization and calibration for (177)Lu quantitative SPECT (QSPECT) with dead-time correction. EJNMMI Phys 2020;7(1).

[30] Kletting P, Schimmel S, Hänscheid H, Luster M, Fernández M, Nosske D, et al. The NUKDOS software for treatment planning in molecular radiotherapy. Z Med Phys 2015;25(3):264–74.

[31] Gear JI, Cox MG, Gustafsson J, Gleisner KS, Murray I, Glatting G, et al. EANM practical guidance on uncertainty analysis for molecular radiotherapy absorbed dose calculations. Eur J Nucl Med Mol Imaging 2018;45(13):2456–74.

[32] Andersson M, Johansson L, Eckerman K, Mattsson S. IDAC-Dose 2.1, an internal dosimetry program for diagnostic nuclear medicine based on the ICRP adult reference voxel phantoms. EJNMMI Res 2017;7(1).
[33] Bolch WE, Eckerman KF, Sgouros G, Thomas SR. MIRD pamphlet No. 21: a generalized schema for radiopharmaceutical dosimetry-standardization of nomenclature. J Nucl Med 2009;50:477–84.
[34] Mowlavi AA, Fornasier MR, Mirzaei M, Bregant P, de Denaro M. Analytical functions for beta and gamma absorbed fractions of iodine-131 in spherical and ellipsoidal volumes. Ann Nucl Med 2014;28(8):824–8.
[35] Grošev D, Lončarić S, Huić D, Dodig D. Geometric models in dosimetry of thyroid remnant mass. Nuklearmedizin 2008;47(03):120–6.
[36] Stabin MG, Sparks RB, Crowe E. OLINDA/EXM: the second-generation personal computer software for internal dose assessment in nuclear medicine. J Nucl Med 2005;46:1023–7.
[37] Rosar F, Schön N, Bohnenberger H, Bartholomä M, Stemler T, Maus S, et al. Comparison of different methods for post-therapeutic dosimetry in [(177)Lu]Lu-PSMA-617 radioligand therapy. EJNMMI Phys 2021;8(1).